Topological transition in $Bi_{1\text{-}x}Sb_x$ studied as a function of Sb doping

Fumitaka Nakamura,[1] Yuka Kousa,[2] Alexey A. Taskin,[3] Yasuo Takeichi,[1] Akinori Nishide,[1] Akito Kakizaki,[1]
Marie D'Angelo,[4] Patrick Lefevre,[5] Francois Bertran,[5] Amina Taleb-Ibrahimi,[5] Fumio Komori,[1] Shin-ichi Kimura,[6]
Hiroshi Kondo,[2] Yoichi Ando,[3,*] and Iwao Matsuda[1,†]

[1]*Institute for Solid State Physics, University of Tokyo, Kashiwa, Chiba 277-8581, Japan*
[2]*Faculty of Science and Technology, Keio University, Yokohama, Kanagawa 223-8522, Japan*
[3]*Institute of Scientific and Industrial Research, Osaka University, Ibaraki, Osaka 567-0047, Japan*
[4]*Institut des Nanosciences de Paris, Université Pierre et Marie Curie-Paris 6, CNRS-UMR 7588, 4 place Jussieu, F-75252 Paris, France*
[5]*Cassiopée Beamline, synchrotron SOLEIL/CNRS, BP 48, F-91192 Gif-Sur-Yvette, France*
[6]*UVSOR Facility, Institute for Molecular Science, Okazaki 444-8585, Japan*

Spin- and angle-resolved photoemission spectroscopy measurements were performed on $Bi_{1-x}Sb_x$ samples at $x = 0.04$, 0.07, and 0.21 to study the change of the surface band structure from nontopological to topological. Energy shift of the T and L_s bulk bands with Sb concentration is quantitatively evaluated. An edge state becomes topologically nontrivial at $x = 0.04$. An additional trivial edge state appears at the L band gap that forms at $x > 0.04$ and apparently hybridize with the nontrivial edge state. A scenario for the topological transition mechanism is presented. Related issues of self-energy and temperature dependence of the surface state are also considered.

I. INTRODUCTION

Bismuth-antimony alloy has long been studied for its thermoelectronic properties,[1] and recently it has been vigorously investigated as a topological insulator.[2] A topological insulator is a material realizing a nontrivial topology in the valence-band wave function. While an energy gap is present for the bulk bands, the edge state is gapless and carries spin current that is topologically protected from scattering by a nonmagnetic impurity.[3–5] Three-dimensional materials are theoretically characterized with eight time-reversal-invariant momenta, and they are classified with four topological invariants,[6] $\nu_0; (\nu_1 \nu_2 \nu_3)$. A (111)-crystal surface of $Bi_{1-x}Sb_x$ ($x > 0.07$) or an Sb crystal is in the topologically nontrivial 1;(111) class, while a Bi crystal is in the topologically trivial 0;(000) class. Doping of Sb atoms into a semimetal Bi crystal results in a quantum phase transition to a topologically insulating $Bi_{1-x}Sb_x$ crystal. Recent photoemission experiments have proven its nature as a topological insulator by observing the odd number of band crossings of the edge states at the Fermi level.[2,7] Bulk band energy shift with Sb doping is crucial for Bi to be a topological insulator, but only "indirect" experiments concerning topological insulators, such as transport measurements, have been performed using Sb doping of Bi.[8] Therefore, direct observation of the bulk band shift and the associated evolution of edge-state band dispersions using, for example, photoemission spectroscopy, is needed for comprehensive understanding.

In the present research, we systematically measured the evolution of the electronic structure of $Bi_{1-x}Sb_x$ at different Sb concentrations ($x = 0.04$, 0.07, and 0.21) by momentum- and spin-resolved photoemission spectroscopy to trace the topological transition from Rashba-split trivial surface states to topological surface states. Shifts of the bulk bands with x are quantitatively evaluated. Changes of the surface-state band structure are experimentally determined. The Σ_2 band becomes topologically nontrivial, connecting the bulk T

valence band and the bulk L_a conduction band at around $x = 0.04$. The additional Σ_1' band appears in the L gap above $x = 0.04$. Surface band structures of the topological $Bi_{1-x}Sb_x$ insulator are likely a result of hybridization between nontrivial edge states and trivial surface states, as proposed in previous theoretical research.[9] In the present article, the related issues of quasiparticle lifetime and the thermal effect of the surface state are also discussed.

II. EXPERIMENTS

High-resolution momentum- and spin-resolved photoemission spectroscopy experiments were performed at the CASSIOPEE beamline (SOLEIL, France) and at the BL-19A beamline (KEK-PF, Japan), respectively. Angle-resolved photoemission spectroscopy (ARPES) measurements were performed with a hemispherical photoelectron spectrometer (VG Scienta R4000) at an energy resolution of 18 meV and an angular resolution of $\pm 0.1°$. Linearly and circularly polarized light at photon energies ranging from 14 to 32 eV were used. The spectra were detected under 7×10^{-9} Pa at 4 K, if not specified in the article. Spin- and angle-resolved photoemission spectroscopy (SARPES) measurements were done with a He-I α source and with a hemispheric analyzer (SPECS Phoibos150) equipped with a home-made, high-yield, very-low-energy electron diffraction (VLEED) spin polarimeter.[10,11] The energy and angle resolutions of the analyzer were 50 meV and $\pm 1°$, respectively. The spectra were detected under 3×10^{-8} Pa at 130 K. The effective Sherman function was $S_{\text{eff}} = 0.29 \pm 0.04$, which was calibrated in advance with the spin polarization of secondary electrons from Ni(110). $Bi_{1-x}Sb_x$ crystals were grown from a stoichiometric mixture of 99.9999% purity Bi and Sb elements by a zone-melting method. $Bi_{1-x}Sb_x$ samples with $x = 0.04$, 0.07, and 0.21 were used in this experiment. The crystals were cleaved along the (111) plane below 130 K. The Sb composition of the surface
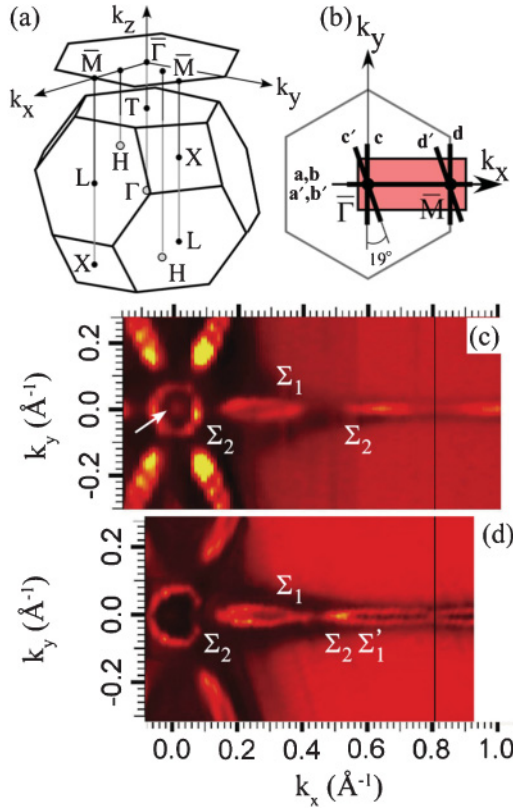
FIG. 1. (Color online) (a) Three-dimensional Brillouin zone and its projection onto the (111) surface. High-symmetry points in the (surface) Brillouin zones are indicated. (b) The surface Brillouin zone (SBZ) is depicted for the measured region in (c) and (d). Thick lines, labeled alphabetically, are the directions of angle-resolved photoemission data shown in the following figures. (c) and (d) are Fermi surfaces of $Bi_{1-x}Sb_x$ at (c) $x = 0.04$ and (d) $x = 0.21$, taken at $hv = 29$ eV. The black solid line corresponds to the zone boundary. Circularly polarized light was used in (c), and linearly polarized light in (d).

was checked with electron-probe microanalysis (EPMA), showing lateral compositional homogeneity over the length scale of the photon beam size for the ARPES measurements. The crystal orientations were determined by *ex situ* x-ray diffraction, *in situ* low-energy electron diffraction (LEED), and by photoemission Fermi surface mapping. Figure 1 shows the normalized photoemission intensity distribution at the Fermi level (± 5 meV) of $Bi_{1-x}Sb_x$ for $x = 0.04$ [Fig. 1(c)] and $x = 0.21$ [Fig. 1(d)], obtained with photon energy $hv = 29$ eV. The spectral features indicated by arrows and labels are described below.

III. RESULTS AND DISCUSSION

A. Sb dependence of $Bi_{1-x}Sb_x$ electronic structure of bulk and surface-state bands

Figures 2(a) and 2(b) show a series of ARPES spectra and the gray-scale band diagram of $Bi_{1-x}Sb_x$ ($x = 0.04$) taken along the $\overline{\Gamma}-\overline{M}$ direction, or k_x axis. The measurement directions for Fig. 2 are indicated in Fig. 1(b). Prominent peaks at $\overline{\Gamma}$ are assigned to the bulk band (**b**), and the spectral tail, extending to the Fermi level (E_F), has created intensity in the

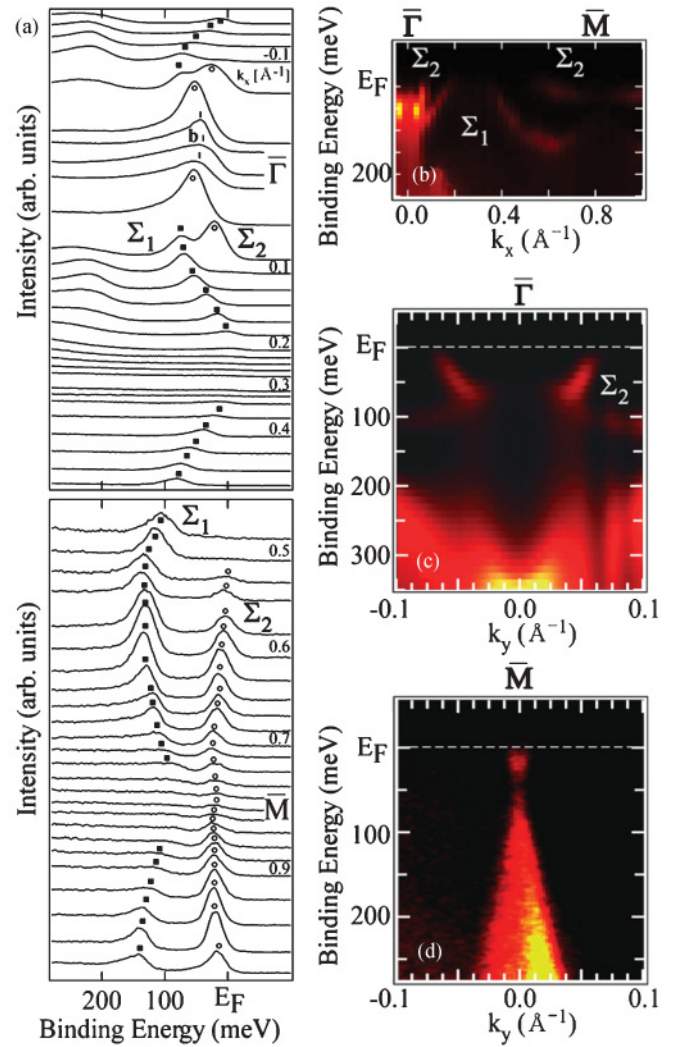FIG. 2. (Color online) A collection of ARPES spectra of $Bi_{1-x}Sb_x$ ($x = 0.04$). The data, taken along the a, b, c, and d lines in the SBZ in Fig. 1(b), are presented in (a), (b), (c), and (d), respectively. Data were obtained at $hv = 29$ eV (circularly polarized light). Peak positions of the edge state (surface state) and bulk bands are marked with symbols.

photoemission Fermi surface as indicated by the white arrow in Fig. 1(c). The assignment of the bulk band was confirmed by observing band dispersion along the k_z direction by changing photon energy. Figure 2(c) displays the photoemission band diagram along the k_y axis around $\overline{\Gamma}$. The Σ_1 and Σ_2 states, identified in the figures, lose photoemission intensity as they disperse in the bulk band region at $\overline{\Gamma}$. This is due to matching of the surface state with the bulk state, forming surface resonance. This causes the lifetime of a hole, created by photoemission process, to be short, resulting in suppression of photoemission intensity. These spectral features indicate that the maximum of the bulk valence band (T band[1]) at $\overline{\Gamma}$ is located nearly at E_F.

Along the $\overline{\Gamma}-\overline{M}$ direction, as shown in Figs. 2(a) and 2(b), two surface states Σ_1 and Σ_2 around $\overline{\Gamma}$ shift to lower binding energy (E_B) as k_x increases, and they cross E_F. Then Σ_1 and Σ_2 reappear at E_F at $k_x \sim 0.35$ and 0.5 Å^{-1}, respectively.

The Σ_2 band moves to higher binding energy as it approaches $\overline{M}$, while the Σ_1 band presents a shallow bottom around $k_x \sim 0.6$ Å^{-1}. As shown in Fig. 1(c), Fermi surfaces of the Σ_2 band are a hexagonal electron pocket at $\overline{\Gamma}$ and oval electron pockets along the $\overline{\Gamma}$–$\overline{M}$ axis, while those of the Σ_1 band are oval hole pockets also along the $\overline{\Gamma}$–$\overline{M}$ axis. At the $\overline{M}$ point, as shown in Fig. 2(d), a Dirac cone with a large Fermi velocity is observed with the energy gap.[12] The lower band can be assigned to the bulk L_s band. Since the binding energy of the Σ_2 band shown in Fig. 2(a) is about 25 meV, which is lower than the gap at 50 meV, the upper band of the Dirac cone is likely the bulk L_a band, which is connected with the dispersion curve of the Σ_2 band. The matching of the edge state with the bulk state is ascertained by reduction of its photoemission intensity at $\overline{M}$.

Figure 3(a) shows a sequence of ARPES spectra of Bi$_{1-x}$Sb$_x$ ($x = 0.21$) taken along the $\overline{\Gamma}$–$\overline{M}$ (k_x) direction. In contrast to
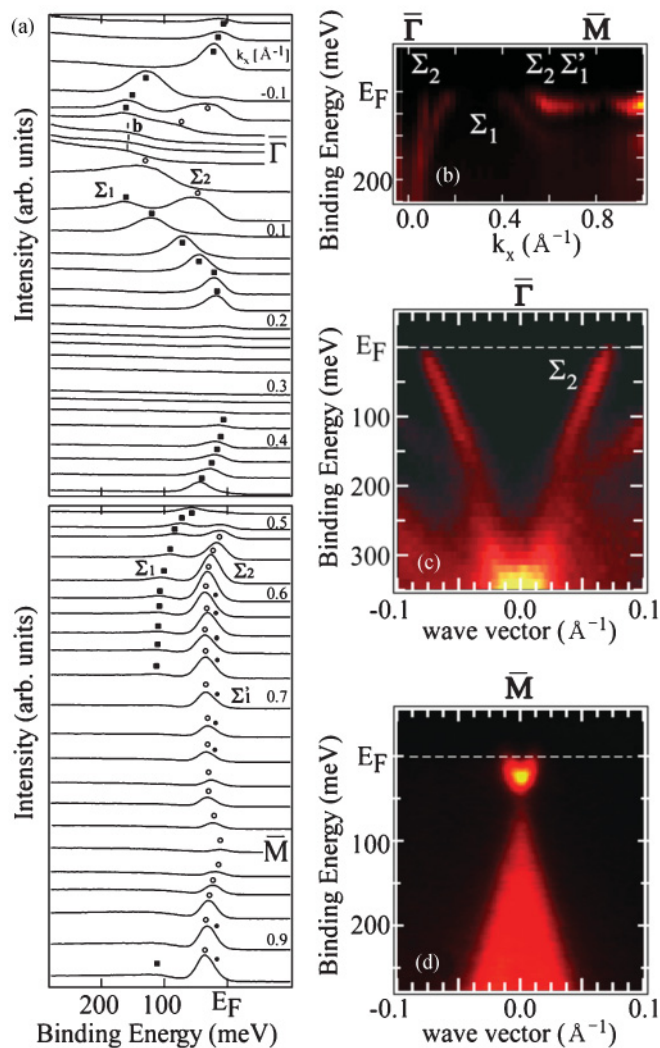
FIG. 3. (Color online) A collection of ARPES spectra of Bi$_{1-x}$Sb$_x$ ($x = 0.21$). The data, taken along a', b', c', and d' lines in the SBZ in Fig. 1(b), are presented in (a), (b), (c), and (d), respectively. Data were obtained at $h\nu = 29$ eV (linearly polarized light). Peak positions of the edge state (surface state) and bulk bands are marked with symbols.

Fig. 2(a), one finds little intensity near E_F at $\overline{\Gamma}$ in Fig. 3(a). Absence of the bulk band indicates a larger energy gap at $\overline{\Gamma}$, and thus the dispersion curve of the Σ_2 surface state is much clearer, as shown in Fig. 3(b). Dispersions of the Σ_1 and Σ_2 bands along the $\overline{\Gamma}$–$\overline{M}$ axis in Fig. 3(a) are similar to those of the $x = 0.04$ sample in Fig. 2(a). Additionally, the Σ_1' band was observed as having peak shoulders near the $\overline{M}$ point. Its existence was verified by detailed comparisons among the ARPES spectra and by peak fitting with Voigt functions. Figure 4(a) shows ARPES spectra at $\overline{M}$ of Bi$_{1-x}$Sb$_x$ crystals at $x = 0.04$ and $x = 0.21$, indicating that both peaks are of the same width. On the other hand, at $k_x = 0.7$ Å^{-1} [Fig. 4(b)], the spectral width of the $x = 0.21$ sample is broader than that of the $x = 0.04$ one. This indicates existence of two edge states in the $x = 0.21$ spectrum, which is not inconsistent with the observation of a single peak at time-reversal-invariant momentum ($\overline{M}$). To trace the two edge states Σ_2 and Σ_1' near E_F, the ARPES spectra of the $x = 0.21$ crystal around $\overline{M}$ are curve fitted with Voigt functions. The Gaussian width was set at 18 meV, corresponding to the total experimental resolution. The Lorentzian width was determined from the ARPES spectra of the $x = 0.04$ sample [Fig. 4(c)] and from the spectrum of the $x = 0.21$ sample at the $\overline{M}$ point. The Fermi-Dirac function is also included in the fit. As shown in Fig. 4(d), each spectrum is well fitted. The Σ_1' band appears and merges with the Σ_2 band at the $\overline{M}$ point. In Fig. 1(d), Fermi surfaces of a hexagonal electron pocket at $\overline{\Gamma}$ and oval hole pockets are assigned to Σ_2 and Σ_1, respectively. The oval Fermi surfaces of electron pockets near $\overline{M}$ originate from the Σ_2 and Σ_1' bands.

Figure 5(a) compares the energy spectra at the Γ point of the three-dimensional BZ ($\overline{\Gamma}$ of SBZ) between the Bi$_{1-x}$Sb$_x$ $x = 0.04$ and 0.21 samples. As described above, a peak at $x = 0.04$ is assigned to the bulk T band, and it shows an energy shift of at least 120 meV (± 30 meV) toward higher binding energy at $x = 0.21$. Figure 5(b) displays ARPES spectra at the $\overline{M}$ point of SBZ for the Bi$_{1-x}$Sb$_x$ $x = 0.04$ and 0.21 samples, also showing higher E_B shift of the spectral bulk band edge with higher Sb concentration. The energy change corresponds to that of the L_s band. Figure 5(c) shows evolution of the bulk band structure of the Bi$_{1-x}$Sb$_x$ alloy as a function of Sb concentration x, estimated in the transport research[1] and evaluated by previous and present photoemission research.[2] Sb doping of the Bi crystal first reduces the energy gap between the two different parity bands L_s and L_a at the L point, and shifts the T band to higher binding energy. Corresponding symmetry points are labeled in Fig. 1(a). Around $x = 0.04$, the L_s and L_a bands cross each other and the gap reopens with inverted ordering. Then the top of the valence band at T comes down further in energy and crosses the bottom of the conduction band at $x = 0.07$. At this point, the indirect gap becomes positive, and the alloy has become an insulator. At $x = 0.09$, the T valence band clears the L_s valence band, and the alloy is a direct-gap insulator at the L points. As x is increased further, the gap increases until it reaches its maximum value at $x = 0.18$. At that point, the valence band at H crosses the L_s valence band. For $x = 0.22$, the H band crosses the L_a conduction band, and the alloy becomes a semimetal again. As indicated in the band diagram
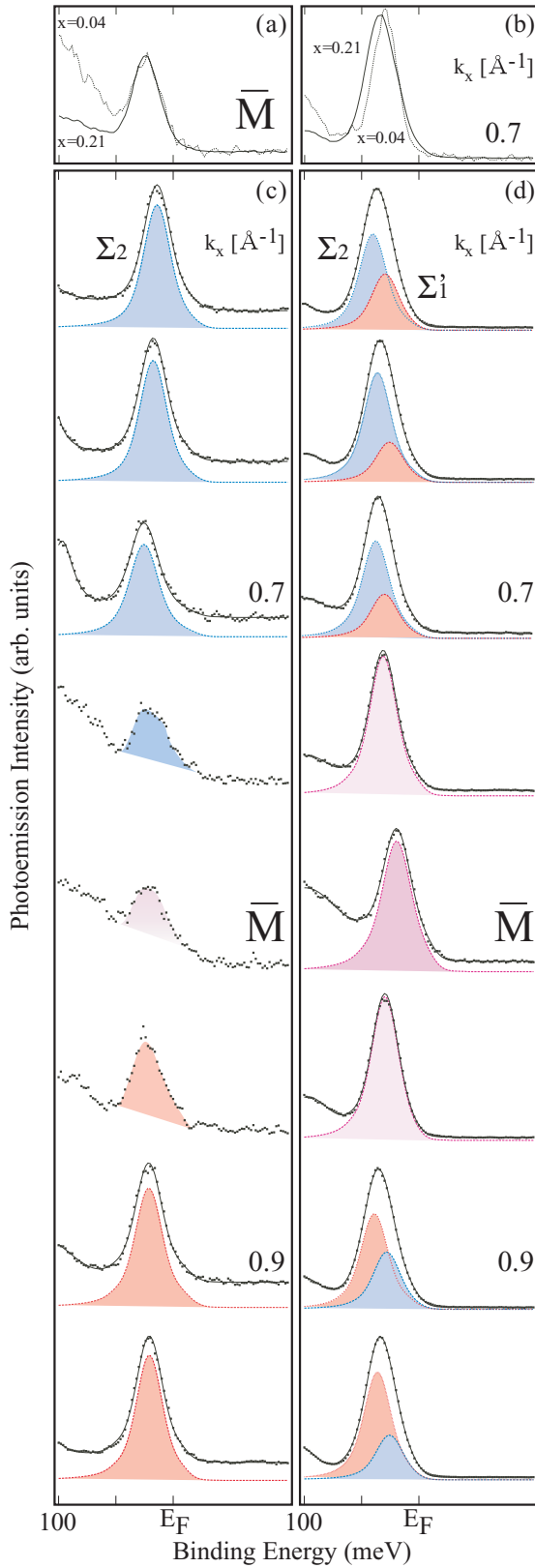
FIG. 4. (Color online) (a) and (b) show ARPES spectra of $Bi_{1-x}Sb_x$ at (a) the $\overline{M}$ point and (b) $k_x = 0.7$ Å^{-1} for the $x = 0.04$ and 0.21 samples, measured at $h\nu = 29$ eV (linearly polarized light). (c) and (d) show a collection of ARPES spectra with the fitted Voigt functions around the $\overline{M}$ point from (c) Fig. 2 and (d) Fig. 3.
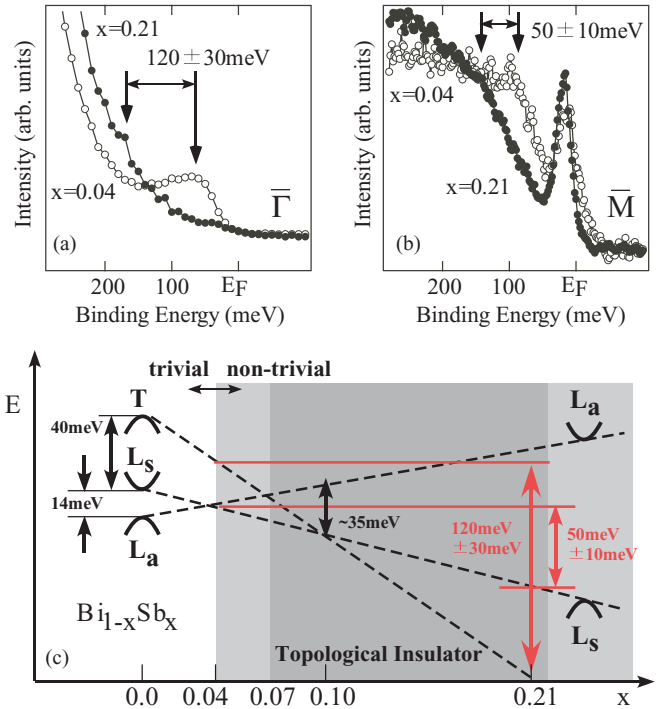

FIG. 5. (Color online) (a) ARPES spectra of $Bi_{1-x}Sb_x$ at $\overline{\Gamma}$ for the $x = 0.04$ and 0.21 samples, measured at $h\nu = 23$ eV (linearly polarized light). (b) ARPES spectra of $Bi_{1-x}Sb_x$ at the $\overline{M}$ point for the $x = 0.04$ and 0.21 samples, measured at $h\nu = 29$ eV (circularly polarized light). (c) Schematic representation[6] of the bulk band energy evolution of $Bi_{1-x}Sb_x$ as a function of x. The energy differences of the bulk bands, evaluated by the present and previous research,[2] are overlapping.

in Fig. 1(a), $Bi_{1-x}Sb_x$ becomes a topological insulator at $x = 0.07$–0.22.

Based on these results, Fig. 6 summarizes the electronic structure of the $Bi_{1-x}Sb_x(111)$ surface at (a) $x = 0.04$ and (b) $x = 0.21$. Around $x = 0.04$, the L_a and L_s bands are likely to close the energy gap and form a Dirac-cone dispersion. The bulk is metallic. Two metallic surface-state bands Σ_1 and Σ_2 exist in the bulk band gap. The Σ_2 band connects to the bulk band at the electron side of the Dirac cone.[12] On the other hand, at $x = 0.21$ the bulk is insulating and three metallic surface-state bands Σ_1, Σ_2, and Σ_1' are identified within the bulk band gap. There exist five E_F crossings of the surface-state band. The odd-number nature classifies $Bi_{1-x}Sb_x$ $(x = 0.21)$ as topologically nontrivial, and thus the material is a topological insulator. These results are consistent with previous photoemission research with different Sb compositions.[2,7,11,13]

B. Spin-polarized surface band structure at $x = 0.07$

It has been reported for $Bi_{1-x}Sb_x(111)$ at $x = 0.0$ and 0.12 that edge states (surface states) of $Bi_{1-x}Sb_x(111)$ are spin split, and that spin-polarized surface band structure occurs over the surface Brillouin zone.[7,11,14] Along the $\overline{\Gamma}$–$\overline{M}$ axis, one spin-up and one spin-down surface-state bands of the Rashba effect were detected for a pure Bi(111) surface,[14]
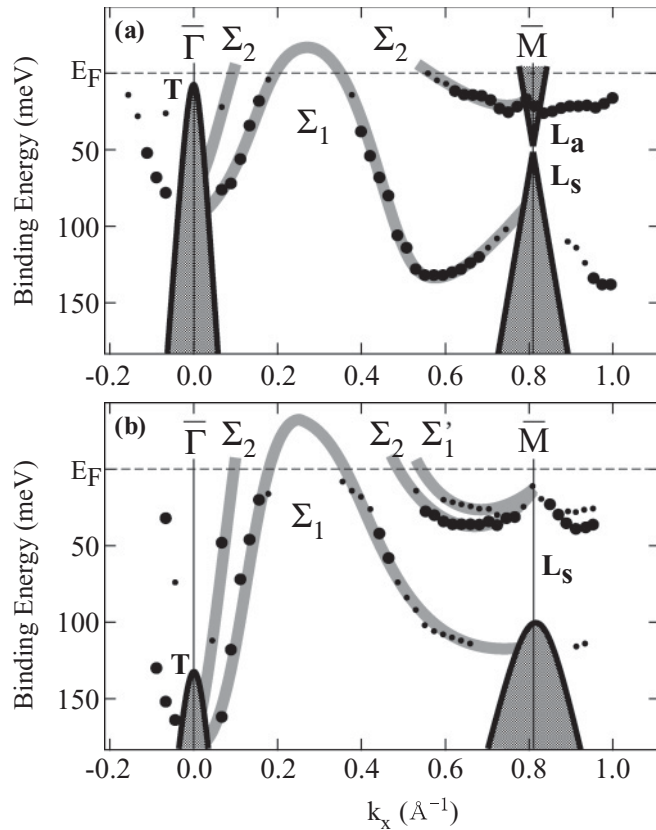
FIG. 6. Spin-integrated photoemission band diagram of Bi$_{1-x}$Sb$_x$ crystals at (a) $x = 0.04$ and (b) $x = 0.21$, determined from ARPES spectra in Figs. 2 and 3. The small and large symbols represent the rather distinctive and the weak spectral features, respectively. The shaded region is the bulk band structure projected onto the SBZ. The edge state and bulk bands are labeled.

while three spin-polarized edge-state bands, i.e., two spin-up and one spin-down, were observed for $x = 0.12$ by spin- and angle-resolved photoemission spectroscopy (SARPES) measurements.[7,11] In order to trace the evolution of the spin structure during the topological transition, SARPES measurements were performed on the Bi$_{1-x}$Sb$_x$(111) surface at an intermediate Sb concentration of $x = 0.07$. Figure 7 shows a series of spin-up and spin-down SARPES measurements along the $\overline{\Gamma}$–$\overline{M}$ direction. Around $\overline{\Gamma}$, spin-up Σ_1 and spin-down Σ_2 bands are identified at positive wave vector (k). Spin characteristics of the two bands are inverted at the opposite k side of $\overline{\Gamma}$ or in the negative wave-vector region. Near $\overline{M}$, one spin-down band, Σ_2, can be identified at k values smaller than the $\overline{M}$ point. The band takes the opposite spin orientation as it passes the $\overline{M}$ point. The previous spin-resolved photoemission research of Bi$_{1-x}$Sb$_x$ at $x = 0.12$ observed both the Σ_2 and Σ_1' bands around $\overline{M}$ with comparable photoemission intensity. The dispersion of the Σ_2 band for $x = 0.07$ suggests that the Dirac point of the surface state, namely, the crossing between the Σ_2 and Σ_1' bands, accidentally coincides with the Fermi energy; this means that the Σ_1' band is located above E_F and is invisible in the present data for $x = 0.07$.
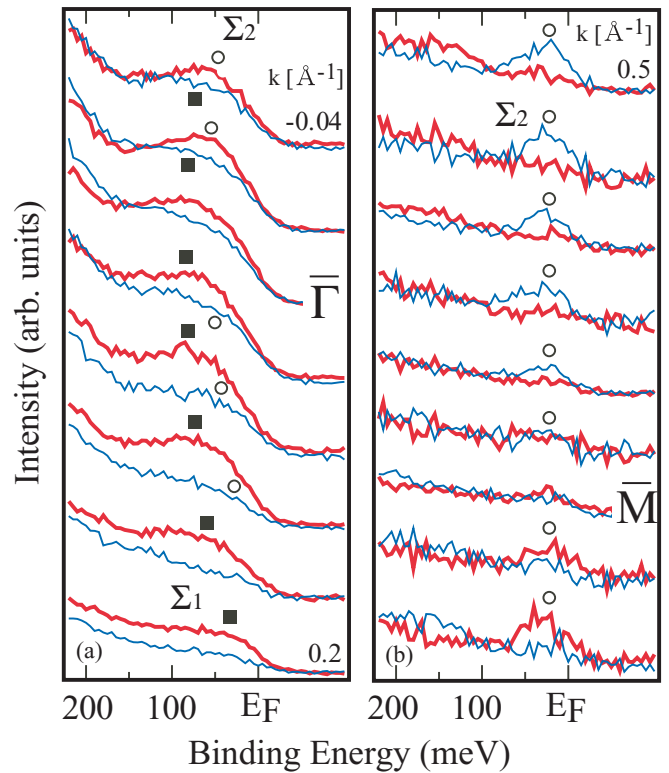

FIG. 7. (Color online) A sequence of SARPES spectra of Bi$_{1-x}$Sb$_x$ ($x = 0.07$) along the $\overline{\Gamma}$–$\overline{M}$ direction. Spin-up and spin-down SARPES data spectra around $\overline{\Gamma}$ and $\overline{M}$ are shown in (a) and (b), respectively. Peak positions of the edge-state (surface-state) bands are marked with symbols.

C. A scenario of the topological transition

From these results, a scenario of the topological transition mechanism of Bi$_{1-x}$Sb$_x$ may be summarized as shown in Fig. 8. For pure Bi ($x = 0.0$), surface-state bands with opposite spin orientations Σ_1 and Σ_2 disperse separately within the bulk band gap, as shown in Fig. 8(a). The Σ_1 and Σ_2 bands connect bulk valence bands of the T band and the L_a band at $\overline{\Gamma}$ and at $\overline{M}$, respectively. Around $x = 0.04$, the bulk L_a and L_s bands
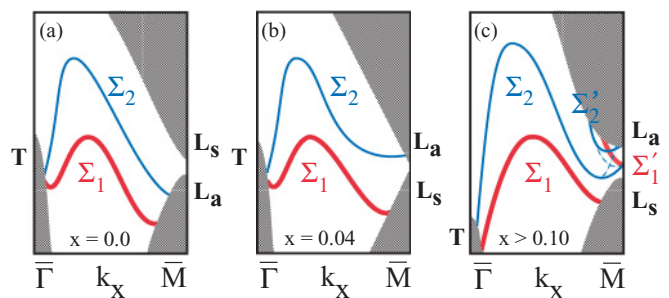

FIG. 8. (Color online) A sequence of surface electronic structure during the topological transition of Bi$_{1-x}$Sb$_x$(111) from the surface Rashba phase to the quantum spin-Hall phase. (a) $x = 0$, trivial pure Bi semimetal with trivial surface states Σ_1 and Σ_2. (b) $x = 0.04$. (c) $x > 0.10$, topological insulator with a nontrivial edge state Σ_2 and trivial edge states Σ_1, Σ_1', and Σ_2', with spin-selective hybridization. The original band dispersions are shown as broken lines.

touch each other, forming a Dirac cone, and then an energy gap is formed between the conduction-band minimum of the L_a band and the valence-band maximum of the L_s band.[12] At this stage the Σ_2 band, being topologically nontrivial, connects the bulk T valence band at $\overline{\Gamma}$ and the bulk L_a conduction band at $\overline{M}$. The change of the surface electronic structure matches the transition mechanism based on the theoretical simulation.[9] Above $x = 0.04$, trivial surface-state bands (Σ_1' and Σ_2') split from the L_a band, are created within the band gap, and are spin polarized due to the Rashba effect. The nontrivial Σ_2 band hybridizes with the trivial Σ_2' band of the same spin orientation. The spin-polarized band structure at $x \geqslant 0.07$ is schematically depicted in Fig. 8(c), which reproduces the band diagram of Fig. 6(b). Detailed dispersion curves of the Σ_1' and Σ_2 bands around the $\overline{M}$ point have been determined for $Bi_{1-x}Sb_x$ crytals at $x = 0.1$[2,13] and also observed at $x = 0.12$ and 0.13.[7,11] The hybridization between the trivial and nontrivial edge states was proposed by theoretical research.[9] The present research suggests that the existence of the trivial states Σ_1' and Σ_2' is likely related to the opening of the inverted gap at the L point.

Creation of a surface state within the bulk band gap has been a long-standing issue in surface science, and there exist various models such as Tamm and Shockley surface states.[15] Recently, a generalized theory was formulated based on the Green-function method.[15] In the linear crystal model, the surface state is formed by the condition

$$|\beta/\alpha_0| < 1, \qquad (1)$$

where β is the resonance integral (matrix element) of the unperturbed bulk Hamiltonian and α_0 is the matrix element of a surface potential. When Eq. (1) is satisfied, the surface energy level lies below (above) the lower (upper) bulk band edge. Based on the model, the magnitude of the surface potential of the $Bi_{1-x}Sb_x(111)$ surface seemingly becomes large with increasing Sb concentration x. The model also suggests that the appearance of the trivial surface states Σ_1' and Σ_2' may depend on surface conditions after crystal cleavage. Theoretical calculations with proper treatment of the surface layer are likely needed to reproduce the band diagrams in Fig. 8(c).

D. Electron-electron interaction of the surface state

High-resolution photoemission results allow us to obtain information on the electron self-energy Σ_{self} that is closely related to the surface band structure. The momentum width of a photoemission-band dispersion curve corresponds to the imaginary part of the electron self energy,[16,17] Im Σ_{self}. Figure 9 shows an example of (a) the photoemission band diagram of the Σ_1 band and (b) the momentum distribution curve (MDC) at $E_B = 50$ meV for the $Bi_{1-x}Sb_x$ ($x = 0.21$) crystal. The MDC data is curve fitted with a Voigt function using the Lorentzian widths as fitting parameters, as shown in Fig. 9(b). The Gaussian width corresponds to the instrumental resolution and it matches the angular resolution of the electron spectrometer, $\pm 0.11°$. The Lorentzian widths (half-width at half-maximum) corresponds to the momentum width that, by multiplication with the band velocity, converts to $|\text{Im }\Sigma_{\text{self}}|$.
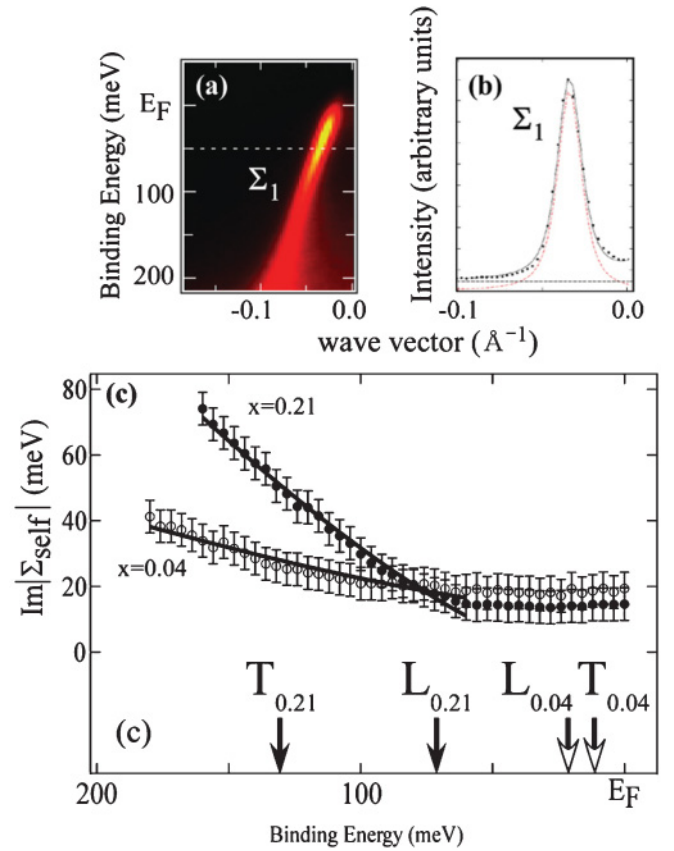

FIG. 9. (Color online) Analysis of the electron self-energy Σ_{self} of the Σ_1 band. (a) Photoemission band diagram of $Bi_{1-x}Sb_x$ ($x = 0.21$) of $k_x = 0.2$ Å^{-1} taken at $h\nu = 29$ eV. The angle scan was taken along an axis rotated 19° with respect to the k_y axis, as shown in Fig. 1(b). (b) Momentum distribution curve at $E_B = 50$ meV, indicated by a broken line in (a). The data were fitted with a Voigt function to obtain the half-width at half-maximum of the peak. (c) Energy dependence of $|\text{Im }\Sigma_{\text{self}}|$ of $Bi_{1-x}Sb_x$ at $x = 0.04$ and 0.21. The bulk band (T and L) edges of each Sb concentration are indicated.

Figure 9(c) shows the dependence of Im Σ_{self} obtained by this procedure with binding energy for $Bi_{1-x}Sb_x$ crystals of the $x = 0.04$ and 0.21 samples. In both cases, a constant $|\text{Im }\Sigma_{\text{self}}|$ of 10–20 meV was obtained from an E_F-to-E_B range of 60 meV, followed by $(E_B)^2$ dependence for $E_B > 60$ meV.

The self-energy of surface-state electrons originates from various process, i.e., electron-phonon coupling, electron-impurity scattering, and electron-electron interaction.[18–21] Electron-electron interaction at a surface is composed of two parts: surface-to-bulk transition and surface-to-surface transition. To consider the former case, edges of the T band and the L band with each Sb concentration are marked in Fig. 9(c). The absence of a systematic energy change at the bulk band maximum indicates that the effect of the surface-to-bulk transition is weak enough to be neglected. The electron-phonon coupling induces discontinuous energy dependence at the Debye energy, and the bulk band transition begins at E_B of the bulk band edge. As shown in Fig. 9(c), no steplike dependence was observed. On the other hand, $|\text{Im }\Sigma_{\text{self}}|$ of the electron-impurity scattering
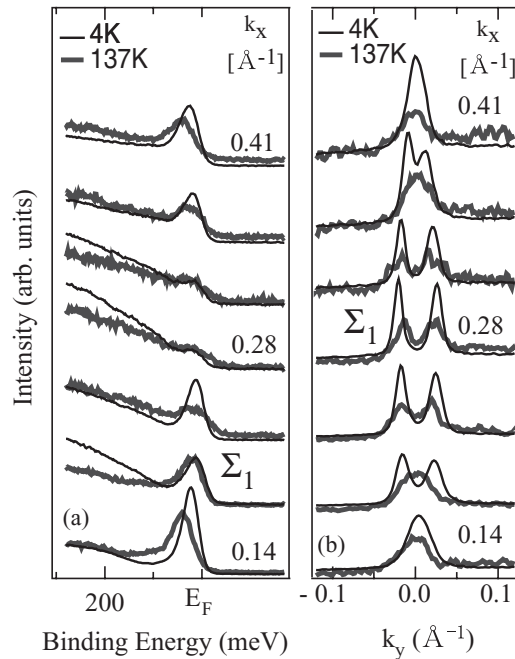
FIG. 10. (a) Energy distribution curves and (b) momentum distribution curves at E_F for Bi$_{1-x}$Sb$_x$ ($x = 0.21$) taken at 137 and 4 K ($h\nu = 29$ eV, linearly polarized light).

has no energy dependence, and that of the electron-electron interaction between the surface-state electrons shows quadratic energy dependence (modified by a logarithmic factor in two-dimensional systems[18]), which were measured in Fig. 9(c). Therefore, the self-energy of the surface-state band of Bi$_{1-x}$Sb$_x$ is dominated by these two process: the electron-impurity scattering below $E_B \sim 60$ meV and the surface state electron-electron interaction above $E_B \sim 60$ meV. The self-energy of the two-dimensional electron-electron interaction, $|\mathrm{Im}\,\Sigma_{\text{el-el}}|$, has been analytically formulated[20,22] as $|\mathrm{Im}\,\Sigma_{\text{el-el}}| = \beta(E_B)^2[\frac{1}{4} + \ln 2 + \frac{1}{2} | \ln(E_B/\mu)|]$, where μ is the Fermi energy for the two-dimensional (surface-state) band. The observed $|\mathrm{Im}\,\Sigma_{\text{self}}|$ data were fitted by the $|\mathrm{Im}\,\Sigma_{\text{el-el}}|$ function [Fig. 9(c)]. Estimating $\mu \sim 200$ meV from the experimental edge-state band dispersions, one crudely obtains $\beta \sim 0.8$ eV^{-1} for $x = 0.04$ and $\beta \sim 2.7$ eV^{-1} for $x = 0.21$. It is important to note that the logarithmic correction factor dominates only at E_F, and it contributes to several percent in the fitted E_B range. Thus, the choice of μ does not alter the present evaluation of the coefficient β. The β value gives a measure of the electron-electron interaction strength and is related to the bandwidth (W) and on-site Coulomb repulsion energy (U) as $2\beta \sim (\pi U^2)/(2W^3)$ within the Born approximation.[18] The width of the Σ_1 band is estimated to be $W \sim 0.2$ eV for $x = 0.04$ and 0.21. From these values, the Coulomb interaction can be estimated to be $U \sim 0.1$ eV for $x = 0.04$ and $U \sim 0.2$ eV for $x = 0.21$. Compared to surface and bulk states of correlated materials,[18,20,23] the Coulomb interaction of the Bi$_{1-x}$Sb$_x$ surface state is much smaller, indicating that electrons at the surface have little electron correlation effect.

E. Temperature dependence of the edge-state band

Finally, we discuss the temperature dependence of the energy position of the edge-state band. Clear E_F crossings of the Σ_1 band were observed in the present photoemission experiment, as shown in Figs. 1–3, whereas those seen in previous research[7,11] were rather obscure. Besides the difference in the Sb concentrations in the samples, the main difference between the experiments was the measurement temperature: $\sim$130 and $\sim$4 K for the previous and the present measurements, respectively. Thus, temperature dependence of the ARPES spectra is examined. Figure 10 shows a series of (a) energy distribution curves and (b) momentum distribution curves (E_F) for Bi$_{1-x}$Sb$_x$ ($x = 0.21$) taken at 4 and 137 K. At $k_x = 0.14$ and 0.41 Å^{-1} in Fig. 10(a), the E_B positions of the Σ_1 state at 137 K are higher than those at 4 K. On the other hand, two peaks in MDCs in Fig. 10(b) indicate two E_F crossings along the k_y axis. The Σ_1 band at 137 K has a smaller k_y range of the double MDC peaks, or smaller Fermi surface, than that at 4 K. The heating and cooling process of the sample was repeated several times to confirm the spectral change with temperature. Then from 4 to 137 K the Σ_1 band was estimated, via EDC and MDC data, to move from 18 ± 4 meV to higher E_B. The direction of the E_B shift with temperature is consistent with the energy position of the band reported at different temperatures,[7,11] as described above. The thermal effect may originate from physisorption of the residual gas or a change in lattice parameter with temperature.[24]

IV. CONCLUSIONS

The spin-polarized electronic structure of Bi$_{1-x}$Sb$_x$ was investigated by spin- and angle-resolved photoemission spectroscopy measurements at Sb concentrations of $x = 0.04$, 0.07, and 0.21. The energy shift of the T and L_s bulk band edge with x was quantitatively evaluated. The topological transition of the surface band structure is likely to be associated with the appearance of a trivial edge state at the L band gap that hybridizes with the nontrivial edge state. A self-energy analysis of the edge state found negligible electron correlation effects at the surface. The energy position of the edge state was found to move to lower binding energy by cooling.

*y_ando@sanken.osaka-u.ac.jp

†imatsuda@issp.u-tokyo.ac.jp

[1] B. Lenoir, M. Cassax, J.-P. Michenaud, H. Scherrer, and S. Scherrer, J. Phys. Chem. Solids **57**, 89 (1996).

[2] D. Hsieh, D. Qian, L. Wray, Y. Xia, Y. S. Hor, R. J. Cava, and M. Z. Hasan, Nature (London) **452**, 970 (2008).

[3] C. L. Kane and E. J. Mele, Phys. Rev. Lett. **95**, 226801 (2005).

[4] C. L. Kane and E. J. Mele, Phys. Rev. Lett. **95**, 146802 (2005).

[5] B. A. Bernevig and S. C. Zhang, Phys. Rev. Lett. **96**, 106802 (2006).

[6] L. Fu and C. L. Kane, Phys. Rev. B **76**, 045302 (2007).

[7] A. Nishide, A. A. Taskin, Y. Takeichi, T. Okuda, A. Kakizaki, T. Hirahara, K. Nakatsuji, F. Komori, Y. Ando, and I. Matsuda, Phys. Rev. B **81**, 041309(R) (2010).

[8] E. I. Rogacheva *et al.*, Appl. Phys. Lett. **94**, 202111 (2009).

[9] H. J. Zhang, C. X. Liu, X. L. Qi, X. Y. Deng, X. Dai, S. C. Zhang, and Z. Fang, Phys. Rev. B **80**, 085307 (2009).

[10] T. Okuda, Y. Takeichi, Yuuki Maeda, A. Harasawa, I. Matsuda, T. Kinoshita, and A. Kakizaki, Rev. Sci. Instrum. **79**, 123117 (2008).

[11] A. Nishide, Y. Takeichi, T. Okuda, A. A. Taskin, T. Hirahara, K. Nakatsuji, F. Komori, A. Kakizaki, Y. Ando, and I. Matsuda, New J. Phys. **12**, 065011 (2010).

[12] P. A. Wolff, J. Phys. Chem. Solids **25**, 1057 (1964).

[13] D. Hsieh, Y. Xia, L. Wray, D. Qian, A. Pal, J. H. Dil, J. Osterwalder, F. Meier, G. Bihlmayer, C. L. Kane, Y. S. Hor, R. J. Cava, and M. Z. Hasan, Science **323**, 919 (2009).

[14] Yu. M. Koroteev, G. Bihlmayer, J. E. Gayone, E. V. Chulkov, S. Blugel, P. M. Echenique, and Ph. Hofmann, Phys. Rev. Lett. **93**, 046403 (2004).

[15] S. G. Davison and M. Steslicka, *Basic Theory of Surface State* (Oxford University Press, New York, 1992).

[16] P. V. Bogdanov, A. Lanzara, S. A. Kellar, X. J. Zhou, E. D. Lu, W. J. Zheng, G. Gu, J.-I. Shimoyama, K. Kishio, H. Ikeda, R. Yoshizaki, Z. Hussain, and Z. X. Shen, Phys. Rev. Lett. **85**, 2581 (2000).

[17] X. J. Zhou *et al.*, Phys. Rev. Lett. **95**, 117001 (2005).

[18] T. Valla, A. V. Fedorov, P. D. Johnson, and S. L. Hulbert, Phys. Rev. Lett. **83**, 2085 (1999).

[19] S. R. Park, W. S. Jung, C. Kim, D. J. Song, C. Kim, S. Kimura, K. D. Lee, and N. Hur, Phys. Rev. B **81**, 041405(R) (2010).

[20] M. Higashiguchi, K. Shimada, M. Arita, Y. Miura, N. Tobita, X. Cui, Y. Aiura, H. Namatame, and M. Taniguchi, Surf. Sci. **601**, 4005 (2007).

[21] V. M. Silkin, T. Balasubramanian, E. V. Chulkov, A. Rubio, and P. M. Echenique, Phys. Rev. B **64**, 085334 (2001).

[22] C. Hodges, H. Smith, and J. W. Wilkins, Phys. Rev. B **4**, 302 (1971).

[23] M. Higashiguchi, K. Shimada, K. Nishiura, X. Cui, H. Namatame, and M. Taniguchi, Phys. Rev. B **72**, 214438 (2005).

[24] S.-J. Tang, H.-T. Jeng, C.-S. Hsue, Ismail, P. T. Sprunger, and E. W. Plummer, Phys. Rev. B **77**, 45405 (2008).